Heliyon 9 (2023) e19057

Contents lists available at ScienceDirect

Heliyon

journal homepage: www.cell.com/heliyon

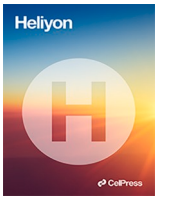

Growth of copper indium diselenide ternary thin films ($CuInSe_2$) for solar cells: Optimization of electrodeposition potential and pH parameters

Armel Ignace N'guessan [a,*], Amal Bouich [a], Donalfologo Soro [b], Bernabé Mari Soucase [a]

[a] Instituto de diseño y Fabricación (IDF), Universitat Politécnica de Valèncía (UPV), Spain
[b] Département des Sciences et Technologie, Ecole Normale Supérieure (ENS) d'Abidjan, Cote d'Ivoire

ARTICLE INFO

Keywords:
Potential
pH
Copper indium diselenium ternary (CISe)
Electrodeposition

ABSTRACT

Herein, copper indium diselenide ternary ($CuInSe_2$) thin film has been deposited on Indium Tin Oxide (ITO) coated glass substrate by electrochemical deposition technique with different potential and pH solutions. $CuInSe_2$ thin films were deposited by one-step electrodeposition before post-depot selenization at 450 °C for 30 min. The effect of potential and pH on the structural and optical properties of CuInSe thin film have been studied using X-ray diffraction (XRD), Scanning electron microscopy (SEM), and UV–Visible spectrometer. According to the X-ray diffraction (XRD) measurements, it was observed that all samples exhibit prominent reflections (112), (204/220), and (312/116) of tetragonal $CuInSe_2$. The films electrodeposited at −0.8 V potential shows growth and peak values increasing in the (204/220) crystal direction within a pH range of 2.2, whereas the films electrodeposited at pH 2.6 tend to favor an increase in (112) peaks. We also noticed an improvement in surface morphology and adherent of $CuInSe_2$ thin films electrodeposited at −0.8 V applied potential from the solution having pH 2.6. The band gaps of samples electrodeposited at −0.8V potentials from pH 2.6, 2.4, and 2.2 solutions were 1.15 eV, 1.25 eV, and 1.21 eV, respectively. As part of our investigation, we used a Solar Cell capacitance simulator (SCAPS) to perform our electrodeposited films. The most effective Power conversion efficiency (PCE) was obtained for thin films electrodeposited at −0.8 V within the solution having pH 2.4.

1. Introduction

CIGS-based thin-film solar cells are continuously being explored to improve thin-film solar cell efficiency. New records in terms of efficiency and productivity are achieved almost every year. The Centre for Solar Energy and Hydrogen Research Baden-Württemberg (ZSW) has improved its thin film CIGS record power conversion efficiency (PCE) of 0.9% from the previous value of 20.8% in 2014 [1]. The latest Solibro published record is 18.72% CIGS module efficiency on a 0.94 m^2 [2]. In 2019, Solar Frontier K.K. achieved a record power conversion efficiency of 23.35% on a 1 cm^2, exceeding the 22.9% achieved in 2017 [3]. These reported values remain quite close to the result obtained from the crystalline silicon solar cell, which is about 26.7% for crystalline silicon cells [4]. In these solar cells, CIGS absorbers can absorb over 90% of solar radiation with a thickness of only 2–3 μm and even with a thickness of 1 μm [5].

* Corresponding author.
E-mail address: amosphysique07@gmail.com (A.I. N'guessan).

https://doi.org/10.1016/j.heliyon.2023.e19057
Received 5 May 2023; Received in revised form 7 August 2023; Accepted 9 August 2023

There are different phases of this alloy depending on the growth conditions. The substrate, element flux, and temperature are some of the parameters that affect the phases and properties of the alloy during growth. The high efficiency of these materials was generally produced using vacuum techniques. However, CuInSe and $Cu(In_{1-x}Ga_{1-x})(S,Se)_2$ thin films are classified as photovoltaic materials with a low-cost elaboration because of the large variety of deposition techniques with high-efficiency including non-vacuum technique such as spray pyrolysis, spin coating, and electrodeposition [5–10]. Electrodeposition is a suitable process for growing an economically large area of CIGS thin film. Electrodeposited Cu–In–Se layers have achieved efficiencies up to 14% for a small area and efficiencies exceeding 11% for a large area [11]. The Deposition of CIS and CIGS absorber layer can be electrodeposited in one set or by two sets [12,13]. However, several parameters such as electrolyte composition, deposition pH and the potential need to be controlled to obtain adequate thickness and good structural and optical properties of deposited thin films. Changing these parameters leads to a significant variation in the material properties. In the case of one set process, these parameters need to be adjusted using complexing agents so that all metal precursors' reduction potential becomes closer [14]. The two-step process involves the deposition of pure elements or combinations with binary or ternary stacked films structure, followed by the selenization or sulfurization of the films [12,15].

The majority of studies have examined the co-deposition (one-step) potential of elements, but very few have examined subsequently the impact of both pH and applied potential on the crystal orientation, optical band gap, and solar cell performance on $CuInSe_2$ thin films electrodeposited [16–18]. In this work, we investigate the effects the effect of potential and pH on the structural and optical properties of $CuInSe_2$ (CISe) absorber layer after co-deposition (one-step) Cu–In–Se layers and selenization. We also exhibit optical bandgap parameters and performed the solar cell by using SCAPS 1-D.

2. Experimental method

$CuInSe_2$ (CISe) films are grown on tin oxide (ITO) coated glass substrate. The electrochemical deposition technique has been used by applying a different value of potential and pH. The electrochemical setup consists of a tin oxide-coated glass substrate (ITO), an Ag/AgCl electrode, and a platinum (Pt) electrode used as working, reference, and counter-electrodes respectively. The substrates were pretreated with 2 ml of Hellmanex III dissolved in distilled water and sonicated for 15 min in acetone, ethanol, and isopropanol. Subsequently, the substrates were dried and finally subjected to UV light in a UV ozone cleaner for 15 min. Different electrolytic baths containing 2.10^{-3} M copper chloride ($CuCl_2$), 10.10^{-3} M indium tri-chloride ($InCl_3$), 4.10^{-3} M selenous acid (H_2SeO_3) in an aqueous solution were prepared. Potassium thiocyanate KSCN (0.04 M), lithium chloride LiCl (0.3 M), and ammonium chloride NH_4Cl_2 (0.1 M) mixed electrolytes were used as a complexing agent, supporting electrolyte and brightener respectively. Potassium hydroxide (KOH) was used to adjust the pH of the bath at different deposition potentials (−0.7 V, −0.8 V, and −0.9 V). The electrodeposition process was performed for 60 min at room temperature. The optimization of the co-deposition process leads us to maintain the potential at −0.8V for different pH values 2.2 (set A), 2.4 (set B), and 2.6 (set C). The as-deposited films were annealed for 30 min at 450 °C in a tubular furnace under a selenium atmosphere and subsequently used for further characterization. Electrodepositing CISe involves the exchange of 13 electrons based on the following reaction (1):

$$Cu^{2+} + In^{3+} + 2SeO_3{}^{2-} + 12H^+ + 13e^- \rightarrow CuInSe_2 + 6H_2O \quad (1)$$

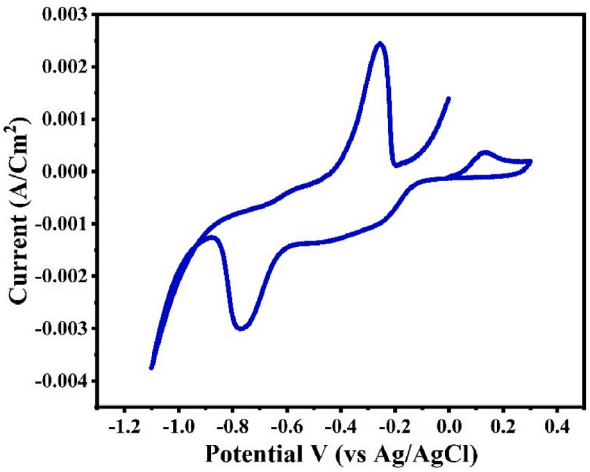

Fig. 1. $CuInSe_2$ CV in combined precursor baths.

3. Results and discussion

3.1. Cyclic voltammetry

Fig. 1 shows the cyclic voltammetry (CV) of $CuInSe_2$ aqueous solution in ambient temperature. The cathodic peak at −0.78 V is attributed to the reduction of the precursor bath as shown in equation (1) with a pH of around 2.4, demonstrating that $CuInSe_2$ can be successfully deposited on an ITO-based glass substrate. In order to analyze the impact of both pH and applied potential various batch of solutions has been prepared, and Potassium hydroxide (KOH) was used to adjust the pH values (2.2, 2.4, and 2.6) at different applied potentials (−0.7 V, −0.8 V, and −0.9 V).

3.2. Structural measurements

The crystallinity with different applied potential and pH values can be seen in the XRD results shown in Fig. 2a and b, and 3. The peaks identified with (#) indicate peaks from ITO substrate. It is seen that the preferential orientation (112) of $CuInSe_2$ can be seen in all samples. At −0.7V, similar peak intensity is observed for the CISe (112) peak at pH 2.4, as seen at pH 2.2, where the In_2Se_3 (InSe) phase can also be observed. At −0.8V, peak intensities are more significant with a growing film in the CISe (112) direction at pH 2.4. Furthermore, the planes (204/220), and (116/312) of CISe appear in all electrodeposited films at −0.8 V deposition potential. At −0.9V, similar behavior can be observed at −0.8 v and −0.7 v for pH values 2.2 and 2.4 respectively.

We found that as well as the pH of the bath remaining constant, the peaks vary with the deposition potential, and increasing applied potential leads to poor adherence of as-deposited films. We observed that the crystallinity tends to improve for −0.8V, and −0.9V with binary InSe and Cu_3Se_2 (CuSe) phases (JCPDS No. 85–0184, JCPDS No. 86–1240), and more preferential orientation peaks for −0.8V [19].

Based on this analysis, the deposition potential has been fixed to −0.8V (vs. SCE). In order to analyze the impact of pH on deposition setup and electrodeposited film properties different solutions of 2.2, 2.4, and 2.6 pH values were prepared. It is observed from Fig. 3 that the intensity of some of the peaks changes with pH. Cu, In, and Se co-deposition potentials at −0.8V lead to film growing in the preferential direction (112) when the pH value changes from 2.2 to 2.6 as reported in Refs. [20–22]. XRD results indicate that typical peaks of the chalcopyrite structure, (112), (204/220), and (312/116) start showing up in the sample deposited at a pH value of 2.4. As the pH of the bath changes, the intensity of these peaks increases, with a strong peak in the (112) preferential orientation without any secondary phases at 2.6 pH. $CuInSe_2$ films electrodeposited at pH 2.4 show growth and increased crystallinity in (204/220) crystal direction whereas the films electrodeposited at pH 2.6 depict the direction along (112).

3.3. FWHM and crystal size

The crystallinity parameters of $CuInSe_2$ thin films electrodeposited at potentials −0.8 V from the solution having pH 2.2 (set A), 2.4

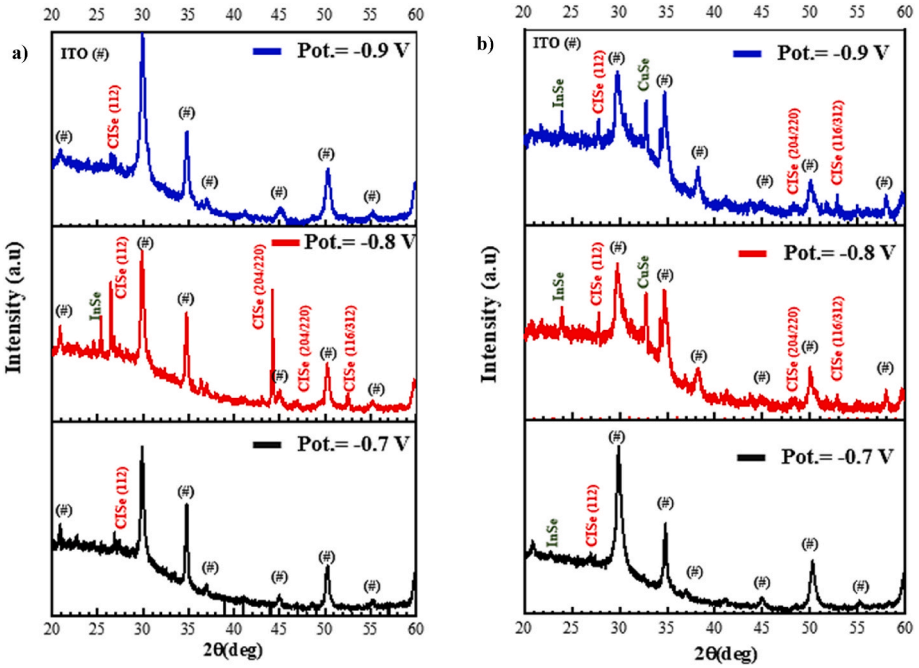

Fig. 2. XRD patterns of electrodeposited CISe thin films with pH (a) 2.4 and (b) 2.2 at −0.7 V, −0.8 V, and −0.9V applied potential.

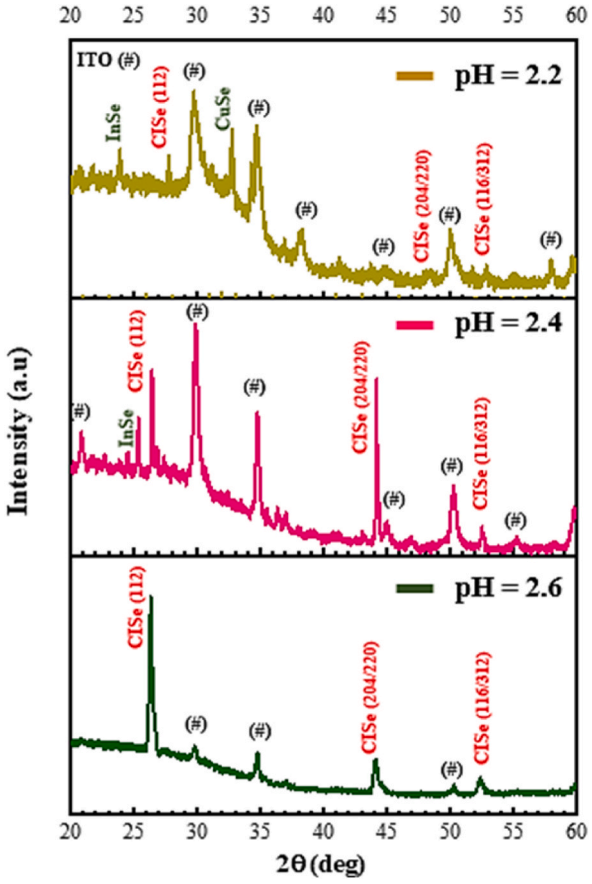

Fig. 3. XRD patterns of $CuInSe_2$ thin films electrodeposited at −0.8 V applied potential from 2.2, 2.4, and 2.6 pH solution.

(set B), and 2.6 (set C) were obtained from XRD results, as shown in Table 1.

Based on the grain size, we can determine the dislocation density per unit volume of the crystal using equations (2) and (3) from Williamson and Smallman [20,23]:

$$\delta = \frac{1}{D^2} \tag{2}$$

The grain deformation ε of the films is examined according to the β values obtained for each angle according to equation (3) [24]:

$$\varepsilon = \frac{\beta}{4 \tan \theta} \tag{3}$$

3.4. Morphology and distribution of elements

Fig. 4a, b, 4c, and 5 show the SEM images and X-ray Energy Dispersive Spectroscopy (EDS) elemental mapping of $CuInSe_2$ thin films electrodeposited at potentials −0.8 V from the solution having pH 2.2 (set A), 2.4 (set B), and 2.6 (set C) with the presence of others

Table 1
Crystal parameters of $CuInSe_2$ thin films electrodeposited at potentials −0.8 V from the solution having pH 2.2 (set A), 2.4 (set B), and 2.6 (set C).

Samples ID	2 theta	hkl	β(FWHM)	d (Ang)	D (nm)	$\delta \times 10^{-3}$ (nm^{-2})	$\varepsilon \times 10^{-3}$
Set A	26.76	112	0.22	3.33	39.40	0.64	23.13
	44.73	204/220	0.94	2.02	9.50	11.08	57.14
Set B	26.79	112	0.12	3.32	70.70	0.20	12.60
	44.19	204/220	0.06	2.04	138.00	0.05	3.70
	52.53	116/312	0.16	1.74	57.00	0.31	8.11
Set C	26.34	112	0.24	3.38	35.30	0.80	25.65
	44.05	204/220	0.35	2.05	25.60	1.52	21.64
	52.39	116/312	0.44	1.74	21.10	2.24	22.37

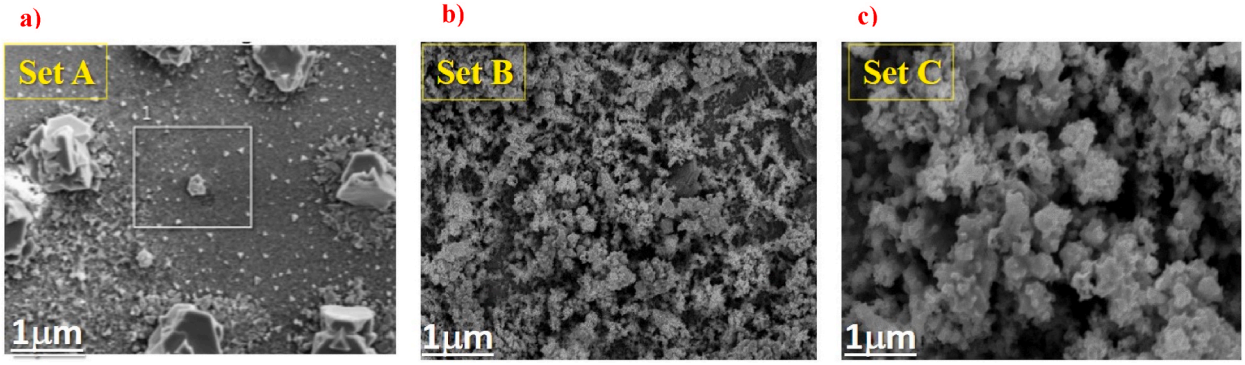

Fig. 4. SEM image of Cu–In–Se layers electrodeposited at potentials −0.8 V from the solution having pH a) 2.2 (set A), b) 2.4 (set B), and c) 2.6 (set C).

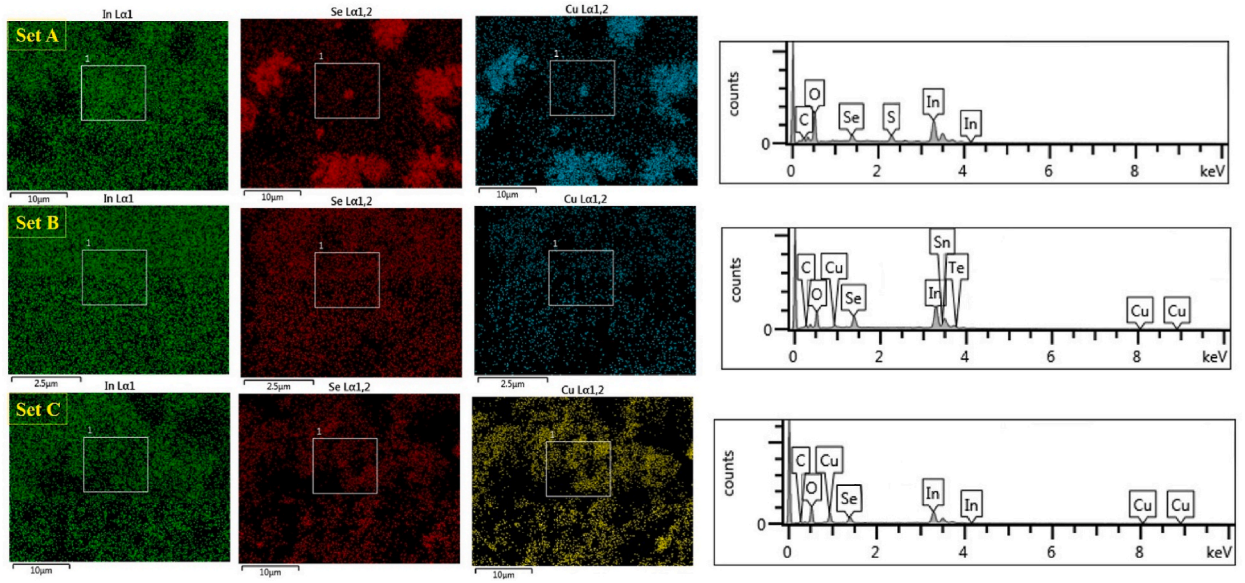

Fig. 5. SEM image and EDS elemental mapping of Cu–In–Se layers electrodeposited at potentials −0.8 V from the solution having pH 2.2 (set A), 2.4 (set B), and 2.6 (set C).

elements (O, C, S …). The improvement in surface morphology and the growth process is evident in Fig. 5 when the pH increases from 2.2 to 2.6.

Table 2 shows the elemental concentrations of each Cu, In, and Se elements for $CuInSe_2$ thin films electrodeposited at −0.8 V applied potentials with 2.2, 2.4, and 2.6 pH values.

The electrodeposition thin films at 2.2, and 2.4 pH values are highly rich in indium as determined by EDS, in agreement with XRD which can be associated to the electrolytic bath composition. However, as pH increases Cu and Se concentrations become more important so that the stoichiometry of the CISe layer is improved. This could be associated to the improvement of complexing agents' ability to form complexes and the adjustment of the reduction potential of precursors [22].

Table 2
Chemical composition of $CuInSe_2$ thin films electrodeposited at potentials −0.8 V from the solution having pH 2.2 (set A), 2.4 (set B), and 2.6 (set C) from Energy-dispersive X-ray Spectroscopy (EDS).

pH of the bath	Potential applied (V)	Atomic percentages (%)		
		Cu	In	Se
2.2 (set A)	−0.8	3.12	85.26	11.62
2.4 (set B)		9.31	71.86	18.83
2.6 (set C)		12.89	68.42	18.74

3.5. Optical proprieties $CuInSe_2$

UV–vis spectrophotometer was used to record $CuInSe_2$ thin films' electrodeposited absorption and transmittance spectrum in the range of 350–850 nm for a solution having pH 2.2 (set A), 2.4 (set B), and 2.6 (set C) at potentials −0.8 V. Fig. 6a and 6b shows that all the materials have good absorption and transmission in the visible region as an absorber layer.

The bandgap E_g values, as shown in Fig. 7, were obtained from absorption spectra data converted into $(\alpha.h\nu)^2$ vs $h\nu$ plot using the Tauc equation (4) which matches well with other methods used in Refs. [23,24].

$$(\alpha h\nu)^{\frac{1}{n}} = A\left(h\nu - E_g\right) \tag{4}$$

h, A, and ν refer to Planck's constant, a constant, and photon frequency, respectively; n is a constant related to electron transitions. The band gap values were found to be 1.16 eV, 1.38 eV, and 1.26 eV for samples electrodeposited at potentials −0.8 V from the solution having pH 2.6 (set C), 2.4 (set B), and 2.2 (set A), respectively. A similar optical properties behavior of electrodeposited films at different pH values was reported in Refs. [21,22,25,26]. As we can observe, the change in bandgap can be attributed to structural modifications arising as a result of grain growth orientation of CISe films, moreover to secondary phases such as InSe and CuSe [27,28]. This can explain why films deposited at 2.6 to secondary phases show the closest bandgap to values reported in the literature [22,29, 30]. However, the absorption and transmission can be affected an increasing way when the pH decreases from 2.6 to 2.2 [21].

4. Numerical devices performance

4.1. Digital structure

$CuInSe_2$ thin films electrodeposited at different pH values impact both the structural and optical properties. A numerical evaluation of $CuInSe_2$ layers electrodeposited using SCAPS-1D was made in order to further analyze the impact of varying band gaps related to the pH solution. We used the same structure and parameters as SCAPS-1D CIGS (example CIGS.def) solar cells, which consists of the following stacking: back contact/p-$CuInSe_2$/OVC/CdS/ZnO-i/Ag, as shown in Fig. 8. The front of the cell is illuminated under a spectrum of AM1.5G equivalent to a density of 100 mW/cm^2 at 300 K. A list of the SCAPS-1D software simulation parameters included the Table 3 of varying band gap related to the different pH values solution at −0.8 V applied potential.

The solar cell studied in this simulation has front and back contact with four other layers where FTO coated glass substrate is the back contact et Ag the front one modeled in flat bande mode. i-ZnO is a transparent conductive oxide (TCO) with optical transparency of about 90% [31] and worked as a windows layer. In CIGS applications, CdS serves as a buffer layer that transports most incident photons to the CIGS absorber layer [32]. OVC (Ordered Vacancy Compound) OVC layer with a thickness of 15 nm and a higher gap energy than $CuInSe_2$ [33] would reduce interfacial recombination [34,35]. SCAPS solves Poisson equations and continuity equations for one-dimensional electrons and holes based on equations (5) and (6, 7) respectively [36,37]:

$$-\varepsilon_0\varepsilon_r\frac{\partial^2 V(x,t)}{\partial^2 x} = q[p(x,t) - n(x,t) + N_D(x) - N_A(x)] + \sum_{piège}\rho_{piège} \tag{5}$$

$$-\frac{1}{q}\frac{\partial J_n(x,t)}{\partial x} = G(x,t) - R_n(x,t) - \frac{\partial n(x,t)}{\partial t} \tag{6}$$

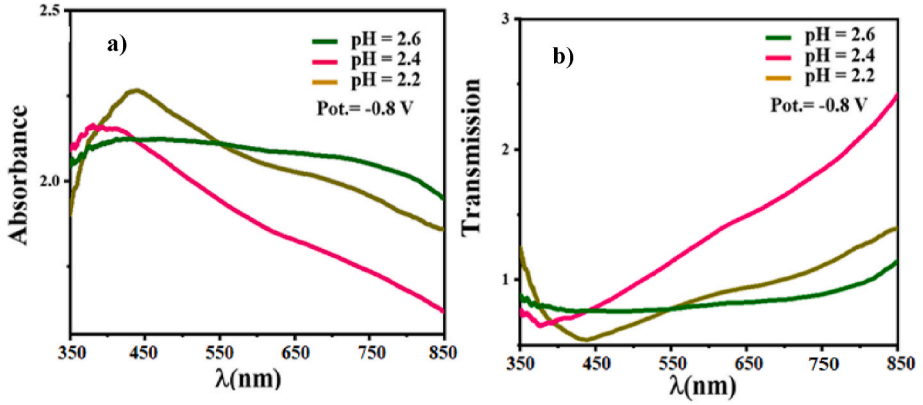

Fig. 6. a) absorbance and b) transmission spectra of $CuInSe_2$ thin films electrodeposited at potentials −0.8 V from the solution having pH 2.2 (set A), 2.4 (set B), and 2.6 (set C).

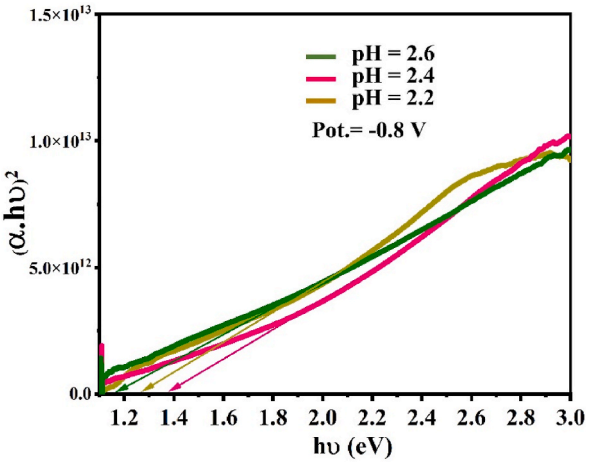

Fig. 7. Optical bandgap $(\alpha.h\nu)^2$ vs $h\nu$ of $CuInSe_2$ thin films electrodeposited at potentials −0.8 V from the solution having pH 2.2 (set A), 2.4 (set B), and 2.6 (set C).

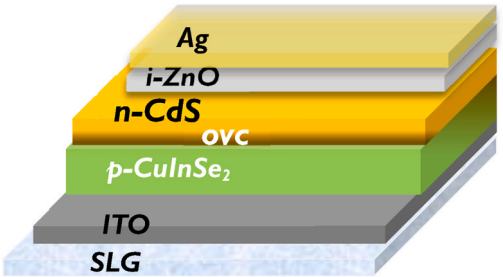

Fig. 8. Schematic of back contact/$CuInSe_2$/OVC/CdS/i-ZnO/Ag Solar Cell.

Table 3
Band gap variation of $CuInSe_2$ thin films electrodeposited at potentials −0.8 V from the solution having pH 2.2 (set A), 2.4 (set B), and 2.6 (set C).

pH of the bath	Potential applied (V)	Bandgap (eV)
		$CuInSe_2$
2.2 (set A)	−0.8	1.26
2.4 (set B)		1.38
2.6 (set C)		1.16

$$\frac{1}{q}\frac{\partial J_p(x,t)}{\partial x} = G(x,t) - R_p(x,t) - \frac{\partial \rho(x,t)}{\partial t} \tag{7}$$

ε_r *and* ε_0 are the relative dielectric and vacuum constants, respectively, V the electric potential, p, and n are the carrier densities, N_A and N_D concentrations of acceptor and donor atoms, J_n and J_p are current densities of electrons and holes, G and $R_{p,n}$ are the generations and recombination rates of holes and electrons. The current density for each type of carrier is given by one-dimensional transport equation (8) and (9):

$$J_n = q\mu_n n\,(x)\varepsilon + qD_n\frac{dn\,(x)}{dx} \tag{8}$$

$$J_p = q\mu_p p\,(x)\varepsilon - qD_p\frac{dp\,(x)}{dx} \tag{9}$$

4.2. *Effect of pH variation on the performances of the devices*

Fig. 9a and b shows J-V and P–V curves for $CuInSe_2$, respectively, and illustrate how varying the pH of $CuInSe_2$ electrodeposited at a

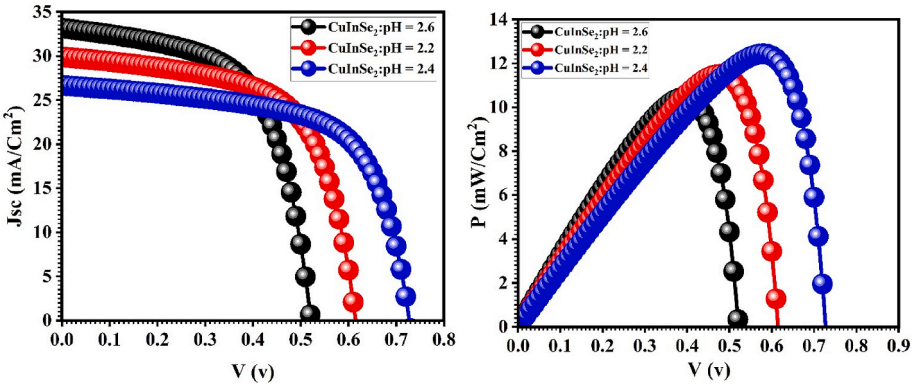

Fig. 9. **a**) J-V and P–V curves of $CuInSe_2$ thin films electrodeposited at potentials −0.8 V from the solution having pH 2.2 (set A), 2.4 (set B), and 2.6 (set C).

constant potential affects the cell's performance. The most efficient current density (Jsc) and power density (P) are obtained when $CuInSe_2$ is deposited at pH 2.4, resulting in the largest band gap (1.38 eV).

The simulation results, as illustrated in Fig. 9 and Table 4, show that the current density (Jsc) decreases as the open circuit voltage (Voc), fill factor (FF), and efficiency (Eta) increase so that when the pH value changes from 2.2 to 2.6 cells' performance was affected by the bandgap. This is indicated by the efficiency of 10.45%, 11.50%, and 12.43% with 1.16 eV, 1.26 eV, and 1.38 eV bandgap at 2.6, 2.2, and 2.4 pH values respectively. Voc and FF are affected in an increasing way by the bandgap whereas Jsc is probably reduced by carrier recombination in the device, particularly at the CISe/OVC/CdS interfaces. Power density or power conversion efficiency increases as long as the bandgap value is closer to the optimal theoretical value (around 1.4 eV) [38–44].

In summary, a pH of around 2.4 is more suitable under the above experimental conditions. This is taking into account the deposition of the $CuInSe_2$ layer and the solar cell's performance [45–47].

5. Conclusion

$CuInSe_2$ thin films were successfully deposited by one-step electrodeposition onto ITO back contact at −07 V, −08V, and −0.9V potential. An aqueous bath with 2.2, 2.4, and 2.6 pH values were used at each applied potential as well and subsequently, the films were selenized at 450 °C for 30 min. According to the X-ray diffraction (XRD) measurements, it was found that $CuInSe_2$ films electrodeposited at −0.8 V potential show growth and increased crystallinity in (204/220) crystal direction from the solution having pH 2.4, whereas the films electrodeposited at pH 2.6, tends to favor the direction along (112) with increasing pH values. Electrodeposited samples from solutions with 2.6, 2.4, and 2.2 pH values showed band gaps of 1.16 eV, 1.38 eV, and 1.26 eV, respectively. The 2.4 pH is more suitable under the above conditions considering the deposition of the $CuInSe_2$ layer and solar cell's performance. The pH of the bath has an impact on the properties of the $CuInSe_2$ electrodeposited film and thus on cell performance.

Author contribution statement

Armel Ignace N'guessan: conceived and designed the experiments; performed the experiments; analyzed and interpreted the data; wrote the paper, Amal Bouich: performed the experiments; Analyzed and interpreted the data; wrote the paper, supervision, Donalfologo Soro: analyzed and interpreted the data, Bernabé Mari Soucase: contributed reagents, materials, analysis tools, or data.

Data availability statement

Data included in article/supplementary material/referenced in article.

Table 4
Experimental Characteristics Parameters of $CuInSe_2$ thin films electrodeposited at −0.8 V applied potential from the solution having pH 2.2 (set A), 2.4 (set B), and 2.6 (set C).

Solar cell model	pH of the bath	Voc (V)	Jsc (mA/cm^2)	FF (%)	Eta (%)
ITO/$CuInSe_2$/OVC/CdS/i-ZnO	2.2 (set A)	0.61	29.91	62.50	11.50
	2.4 (set B)	0.73	26.66	64.09	12.43
	2.6 (set C)	0.52	33.17	60.44	10.45

Declaration of competing interest

The authors declare that they have no known competing financial interests or personal relationships that could have appeared to influence the work reported in this paper.

Acknowledgment

Author Armel Ignace N'Guessan acknowledges his Erasmus+ KA 107, The author Amal Bouich acknowledges the Ministerio de Ciencia e Innovación (Spain) (MCIN) for funding support through Margarita Salas Fellowship (MCIN/AEI/10.13039/501100011033). This work has been funded by the Ministerio de Ciencia e Innovación (Spain) and by the Spanish Agencia Estatal de Investigación through projects BESTMAT PID2019-107137RB-C21/AEI/10.13039/501100011033 and PID2019-107137RB-C22/AEI/10.13039/501100011033 and by ERDF under the funding "A way of making Europe".

References

[1] P. Jackson, D. Hariskos, R. Wuerz, O. Kiowski, A. Bauer, T.M. Friedlmeier, M. Powalla, Properties of Cu(In,Ga)Se2 solar cells with new record efficiencies up to 21.7, Phys. Status Solidi 9 (1) (2015) 28–31, https://doi.org/10.1002/pssr.201409520.
[2] A. Bouich, J.C. Torres, Y.H. Khattak, F. Baig, J. Marí-Guaita, B.M. Soucase, et al., Bright future by controlling α/δ phase junction of formamidinium lead iodide doped by imidazolium for solar cells: Insight from experimental, DFT calculations and SCAPS simulation, Surf. Interfaces 40 (2023) 103159.
[3] M. Nakamura, K. Yamaguchi, Y. Kimoto, Y. Yasaki, T. Kato, H. Sugimoto, Cd-free Cu(in,Ga)(Se,S)2 thin-film solar cell with record efficiency of 23.35, IEEE J. Photovoltaics 9 (6) (2019) 1863–1867, https://doi.org/10.1109/JPHOTOV.2019.2937218.
[4] M.A. Green, Corrigendum to "improved silicon optical parameters at 25°C, 295K and 300K including temperature coefficients" [prog. Photovolt: res. Appl. 2022; 30: 164–179], Prog. Photovolt. 30 (9) (2022) 1144–1145, https://doi.org/10.1002/pip.3560.
[5] L. Tsakalakos, Nanostructures for photovoltaics, Mater. Sci. Eng. R Rep. 62 (6) (2008) 175–189, https://doi.org/10.1016/j.mser.2008.06.002.
[6] Y. Oh, W. Yang, J. Kim, K. Woo, J. Moon, Aqueous solution-phase selenized CuIn(S,Se)2 thin film solar cells annealed under inert atmosphere, ACS Appl. Mater. Interfaces 7 (40) (2015) 22570–22577, https://doi.org/10.1021/acsami.5b06996.
[7] A.R. Uhl, J.K. Katahara, H.W. Hillhouse, Molecular-ink route to 13.0% efficient low-bandgap CuIn(S,Se)2 and 14.7% efficient Cu(In,Ga)(S,Se)2 solar cells, Energy Environ. Sci. 9 (1) (2016) 130–134, https://doi.org/10.1039/C5EE02870A.
[8] W. Septina, M. Kurihara, S. Ikeda, Y. Nakajima, T. Hirano, Y. Kawasaki, T. Harada, M. Matsumura, Cu(In,Ga)(S,Se)2 thin film solar cell with 10.7% conversion efficiency obtained by selenization of the Na-doped spray-pyrolyzed sulfide precursor film, ACS Appl. Mater. Interfaces 7 (12) (2015) 6472–6479, https://doi.org/10.1021/am507684x.
[9] B.J. Babu, S. Velumani, A. Morales-Acevedo, R. Asomoza, Properties of CuInGaSe thin films prepared by chemical spray pyrolysis. https://doi.org/10.1109/ICEEE.2010.5608628, 2010.
[10] S. Aksu, M. Pinarbasi, Electrodeposition methods and chemistries for deposition of CIGS precursor thin films. https://doi.org/10.1109/PVSC.2011.6185907, 2011.
[11] B. Başol, M. Pinarbasi, S. Aksu, J. Wang, Y. Matus, T. Johnson, Y. Han, M. Narasimhan, B. Metin, Electroplating-based CIGS Technology for Roll-To-Roll Manufacturing, 23rd European Photovoltaic Solar Energy Conference, 2008.
[12] A. Duchatelet, T. Sidali, N. Loones, G. Savidand, E. Chassaing, D. Lincot, 12.4% Efficient Cu(In,Ga)Se2 solar cell prepared from one step electrodeposited Cu–In–Ga oxide precursor layer, Sol. Energy Mater. Sol. Cell. 119 (2013) 241–245, https://doi.org/10.1016/j.solmat.2013.07.053.
[13] K. Bouabid, A. Ihlal, A. Manar, A. Outzourhit, E.L. Ameziane, Effect of deposition and annealing parameters on the properties of electrodeposited CuIn1−xGaxSe2 thin films, Thin Solid Films 488 (1–2) (2005) 62–67, https://doi.org/10.1016/j.tsf.2005.04.111.
[14] G. Zangari, Electrodeposition of alloys and compounds in the era of microelectronics and energy conversion technology, Coatings 5 (2) (2015) 195–218, https://doi.org/10.3390/coatings5020195.
[15] D. Lincot, J.F. Guillemoles, S. Taunier, D. Guimard, J. Sicx-Kurdi, A. Chaumont, O. Roussel, O. Ramdani, C. Hubert, J.P. Fauvarque, Chalcopyrite thin film solar cells by electrodeposition, Sol. Energy 77 (6) (2004) 725–737, https://doi.org/10.1016/j.solener.2004.05.024.
[16] M.E. Calixto, K.D. Dobson, B.E. McCandless, R.W. Birkmire, Controlling growth chemistry and morphology of single-bath electrodeposited Cu(in,Ga)Se[sub 2] thin films for photovoltaic application, J. Electrochem. Soc. 153 (6) (2006) G521, https://doi.org/10.1149/1.2186764.
[17] J. Kois, S. Bereznev, E. Mellikov, A. Öpik, Electrodeposition of CuInSe2 thin films onto Mo-glass substrates, Thin Solid Films 511–512 (2006) 420–424, https://doi.org/10.1016/j.tsf.2005.11.075.
[18] M.C.F. Oliveira, M. Azevedo, A. Cunha, A voltammetric study of the electrodeposition of CuInSe2 in a citrate electrolyte, Thin Solid Films 405 (1–2) (2002) 129–134, https://doi.org/10.1016/S0040-6090(01)01720-5.
[19] K.G. Deepa, N. Lakshmi Shruthi, M. Anantha Sunil, J. Nagaraju, Cu(In,Al)Se2 thin films by one-step electrodeposition for photovoltaics, Thin Solid Films 551 (2014) 1–7, https://doi.org/10.1016/j.tsf.2013.10.180.
[20] A.B. Rohom, P.U. Londhe, N.B. Chaure, The effect of pH and selenization on the properties of CuInSe2 thin films prepared by electrodeposition technique for device applications, J. Solid State Electrochem. 19 (1) (2015) 201–210, https://doi.org/10.1007/s10008-014-2582-0.
[21] R. Sani, R. Manivannan, S. Noyel Victoria, One step electrodeposition of copper zinc tin sulfide using sodium thiocyanate as complexing agent, J. Electrochem. Sci. Tech. 9 (4) (2018), https://doi.org/10.5229/JECST.2018.9.4.308.
[22] M.A. Frontini, M. Vázquez, Electrodeposition of CuInSe2 in citrate-containing electrolytes, J. Mater. Sci. 45 (11) (2010) 2995–3000, https://doi.org/10.1007/s10853-010-4300-3.
[23] M.R. Arefi-Rad, H. Kafashan, Pb-doped SnS nano-powders: comprehensive physical characterizations, Opt. Mater. 105 (2020), 109887, https://doi.org/10.1016/j.optmat.2020.109887.
[24] A. Alasvand, H. Kafashan, Investigation the effect of Pb incorporation on the surface characterizations of electrodeposited CdSe nanostructures, J. Alloys Compd. 817 (2020), 152711, https://doi.org/10.1016/j.jallcom.2019.152711.
[25] M.A. Shafi, L. Khan, S. Ullah, A. Bouich, H. Ullah, B. Mari, Synthesis of CZTS kesterite by pH adjustment in order to improve the performance of CZTS thin film for photovoltaic applications, Micro Nanostruc. 164 (2022), 107185, https://doi.org/10.1016/j.spmi.2022.107185.
[26] B. Ananthoju, A. Kushwaha, F.J. Sonia, M. Aslam, Structural and Optical Properties of Electrochemically Grown Highly Crystalline Cu[sub 2]ZnSnS[sub 4] (CZTS) Thin Films, 2013, https://doi.org/10.1063/1.4791233.
[27] T. Satoh, S. Hayashi, S. Nishiwaki, S. Shimakawa, Y. Hashimoto, T. Negami, T. Uenoyama, Fabrication of Cu(In,Ga)Se2 by in-line evaporation (composition monitoring method using heat radiation), Sol. Energy Mater. Sol. Cell. 67 (1–4) (2001) 203–207, https://doi.org/10.1016/S0927-0248(00)00282-8.
[28] S. Fiat Varol, G. Babür, G. Çankaya, U. Kölemen, Synthesis of sol–gel derived nano-crystalline ZnO thin films as TCO window layer: effect of sol aging and boron, RSC Adv. 4 (100) (2014) 56645–56653, https://doi.org/10.1039/C4RA11324A.
[29] M. Valdés, M. Vázquez, A. Goossens, Electrodeposition of CuInSe2 and In2Se3 on flat and nanoporous TiO2 substrates, Electrochim. Acta 54 (2) (2008) 524–529, https://doi.org/10.1016/j.electacta.2008.07.036.
[30] F. Kang, J.P. Ao, G.Z. Sun, Q. He, Y. Sun, Growth and characterization of CuInSe2 thin films via one-step electrodeposition from a lactic acid/sodium lactate buffer system, Mater. Chem. Phys. 115 (2–3) (2009) 516–520, https://doi.org/10.1016/j.matchemphys.2009.02.006.

[31] F. Zhang, C. Sun, C. Bajracharya, R.G. Rodriguez, J.J. Pak, Fabrication and characterization of thin film solar cell made from CuIn0.75Ga0.25S2Wurtzite nanoparticles, J. Nanomater. (2013) 1–5, https://doi.org/10.1155/2013/320375, 2013.
[32] U.P. Singh, S.P. Patra, Progress in polycrystalline thin-film Cu(in,Ga)Se2Solar cells, Int. J. Photoenergy (2010) 1–19, https://doi.org/10.1155/2010/468147, 2010.
[33] S.B. Zhang, S.-H. Wei, A. Zunger, H. Katayama-Yoshida, Defect physics of theCuInSe2chalcopyrite semiconductor, Phys. Rev. B 57 (16) (1998) 9642–9656, https://doi.org/10.1103/PhysRevB.57.9642.
[34] A. Kumar, Efficiency enhancement of CZTS solar cells using structural engineering, Superlattice. Microst. 153 (2021), 106872, https://doi.org/10.1016/j.spmi.2021.106872.
[35] A. Kumar, P. Ranjan, Defects signature in VOC characterization of thin-film solar cells, Sol. Energy 220 (2021) 35–42, https://doi.org/10.1016/j.solener.2021.03.017.
[36] H. Movla, Optimization of the CIGS based thin film solar cells: numerical simulation and analysis, Optik 125 (1) (2014) 67–70, https://doi.org/10.1016/j.ijleo.2013.06.034.
[37] M. Mostefaoui, H. Mazari, S. Khelifi, A. Bouraiou, R. Dabou, Simulation of high efficiency CIGS solar cells with SCAPS-1D software, Energy Proc. 74 (2015) 736–744, https://doi.org/10.1016/j.egypro.2015.07.809.
[38] G. Jarosz, R. Marczyński, R. Signerski, Effect of band gap on power conversion efficiency of single-junction semiconductor photovoltaic cells under white light phosphor-based LED illumination, Mater. Sci. Semicond. Process. 107 (2020), 104812, https://doi.org/10.1016/j.mssp.2019.104812.
[39] A. Bouich, J.C. Torres, H. Chfii, J. Marí-Guaita, Y.H. Khattak, F. Baig, B.M. Soucase, P. Palacios, Delafossite as hole transport layer a new pathway for efficient perovskite-based solar sells: insight from experimental, DFT and numerical analysis, Sol. Energy 250 (2023) 18–32, https://doi.org/10.1016/j.solener.2022.12.022.
[40] Y. Doumbia, A. Bouich, B.M. Soucasse, D. Soro, Boosting the stability and growth of methylammonium lead bromide perovskites film doped with FA for solar cells, Opt. Mater. 137 (2023), 113563, https://doi.org/10.1016/j.optmat.2023.113563.
[41] A. Touré, A. Bouich, B.M. Soucasse, D. Soro, Investigation of the optoelectronics properties and stability of Formamidinium lead mixed halides perovskite, Opt. Mater. 135 (2023), 113334, https://doi.org/10.1016/j.optmat.2022.113334.
[42] N. Bouri, A. Talbi, Y. Khaaissa, S. Derbali, A. Bouich, K. Nouneh, Insight into MAPb1−xEuxI3 based perovskite solar cell performance using SCAPS Simulator, Optik 271 (2022), 170235, https://doi.org/10.1016/j.ijleo.2022.170235.
[43] K.E. Koné, A. Bouich, B.M. Soucase, D. Soro, Manufacture of different oxides with high uniformity for copper zinc tin sulfide (CZTS) based solar cells, J. Mol. Graph. Model. 121 (2023), 108448, https://doi.org/10.1016/j.jmgm.2023.108448.
[44] K.E. Koné, A. Bouich, D. Soro, B.M. Soucase, Insight of ZnO/CuO and ZnO/Cu2O solar cells efficiency with SCAPS simulator, Opt. Quant. Electron. 55 (7) (2023), https://doi.org/10.1007/s11082-023-04892-9.
[45] Y. Doumbia, A. Bouich, D. Soro, B.M. Soucase, Mixed halide head perovskites thin films: stability and growth investigation, Optik 261 (2022) 169222.
[46] Bouich A.. Study and characterization of hybrid perovskites and copper-indium-gallium selenide thin films for tandem solar cells, 2021 (Doctoral dissertation, Universitat Politècnica de València), https://doi.org/10.4995/Thesis/10251/160621.
[47] A.I. N'guessan, A. Bouich, A. Touré, B.M. Soucasse, D. Soro. Influence of Sulfur Content in Zn (O, S) Buffer Layer onto Copper Indium Gallium Sulfur-Based Solar Cells Through SurfaceEngineering at $ZnO_{1-x}S_x$/CIGS Interface, 2023.